2012-01-01

A Generalized Version of an Ivantsov-based Dendrite Growth Model Incorporating a Facility for Solute Measurement Ahead of the Tip

Shaun McFadden
Dublin Insitute of Technology, shaun.mcfadden@dit.ie

David J. Browne
University College Dublin

Recommended Citation

S. McFadden, D.J. Browne, A generalized version of an Ivantsov-based dendrite growth model incorporating a facility for solute measurement ahead of the tip, Computational Materials Science, vol.55, pages 245-254, 2012

Title: A generalized version of an Ivantsov-based dendrite growth model incorporating a facility for solute measurement ahead of the tip

Shaun McFadden[1], David J. Browne[2]

1, School of mechanical and transport engineering, Dublin Institute of Technology, Bolton St, Dublin 1, Ireland

2, School of Mechanical and Materials Engineering, University College Dublin, Belfield, Dublin 4, Ireland

Shaun McFadden (+353 1 4023920) shaun.mcfadden@dit.ie (Corresponding author)

David J. Browne (+353 1 7161901) David.browne@ucd.ie

Keywords

Dendritic growth; Solidification

Abstract

Extensions to the Ivantsov dendrite growth model are presented, which allow for increased solute levels in the field ahead of the dendrite tip. This model is intended for use with video-microscopy experimental results taken from synchrotron radiography sources. Ideally, the composition and composition gradient at the solid-liquid interface would be measured. However, due to the spatial resolution limitations, it is difficult to accurately measure the composition at the interface. This paper sets out an extended description of the theory where measurements ahead of the tip determine the operating conditions at the tip. This extended model of dendritic growth may be incorporated into solidification process models, thus improving predictions where the solute field ahead of the tip may change due to solutal build up from neighbouring dendrites. It is shown that growth arrest is predicted in cases where local solutal enrichment reaches a critical level. A distinction between global and local tip undercooling is made. The usefulness of this model is demonstrated with an application to experimental results for a binary (Al-Ge) alloy.

1. Introduction

Metallic alloys typically solidify as dendritic crystal structures; hence, detailed reviews of dendritic growth models have been written [1,2,3,4]. The dendritic growth models are usually based on the premise of diffusion-controlled transport around a parabolic solid-liquid interface. Ivantsov [5,6] provided the elementary mathematical treatment of the steady-state transport process at the solid-liquid interface by diffusion. Later Horvay and Cahn [7] provided a rigorous mathematical treatment of the steady-state diffusion process around parabolic interfaces with various solid geometries including the 3D paraboloid of revolution, the elliptical paraboloid, and the 2D parabolic plate. In the basic models of Ivantsov and Horvay-Cahn, it is assumed that a boundary condition exists at an infinite distance from the solid-liquid interface where the field parameter is at some nominal value. Hence the Ivantsov and Horavy-Cahn solutions are truly established for isolated dendrites that have no interfering neighbours.

For thermal dendrites growing in a pure substance, it is the transport of heat from the solid-liquid interface that determines the growth rate. Hence, Ivantsov's diffusion transport model has been applied to the temperature field to determine the growth conditions. For solutal dendrites (found in metallic alloys) it is the transport of both solute and heat from the solid liquid interface that determines the growth rate. Lipton, Glicksman, and Kurz [8,9] demonstrated how the Ivantsov mathematical model could be deployed to treat both the heat transport and solute transport problems for unconstrained equiaxed grains. However, Trivedi and Kurz [2] showed that if the temperature field is known or assumed *a priori* (for example, in the directional solidification scenario) then we only need to use the Ivantsov solution to treat the solute transport problem.

An additional selection criterion is required to determine the operating conditions (the combination of radius and growth rate) at the dendrite tip. Stefanescu [10] gives a summary of three selection criteria: the extremum criterion, the marginal stability criterion, and the microsolvability theory. The extremum criterion is seldom used and shall be ignored in this discussion. Both the marginal stability criterion [11,12] and the microsolvability theory [13,14] provide a solution for a tip selection parameter σ^*. The marginal stability calculates the tip selection parameter as $\sigma^* = 1/4\pi^2$. Marginal stability determines that the tip selection parameter is assumed constant for all materials under all conditions. Work has been done to validate growth models of thermal dendrites in organic transparent systems [4] and the marginal stability parameter gives a reasonable approximation of the experimentally-observed growth conditions. Marginal stability is deemed fit for purpose in many cases. However, the marginal stability criterion has no secure physical basis. And empirical evidence [15] has shown that in some cases the measured tip selection parameter deviates significantly enough to warrant further investigation. The microsolvability theory, as described in [10] and [16] , gives a tip selection parameter, σ^*, based on the crystal anisotropy, ε. The microsolavability theory is deemed to be derived from a sounder theoretical basis than the marginal stability theory. Muschol et al. [17] summarised available surface energy anisotropy strength, ε, for transparent alloys and compared with microscopic solvability theory. Differences between theoretical and experimental values for σ^* were demonstrated. Unfortunately, for most metallic alloys there is a lack of credible experimental data for surface energy anisotropy strength. Rebow and Browne [18] discuss a simple scaling law which may be used to estimate the stability parameter based on scaling the crystal anisotropy, ε. Recently Mullis [19] presented results from a phase field model where the tip selection parameter, σ^*, was calculated from the velocity and curvature data. The tip selection was shown to be changing as a function of tip undercooling. Comparisons were made with another model that used the constant value for σ^* based on the marginal stability criterion.

In macro models of solidification, the heat transport problem, or heat equation, is solved numerically. Furthermore, a polynomial expression written in terms of undercooling at the dendrite tip, determined from the Ivantsov solution, may be used to determine the growth rate of the dendrite envelope (see for example [20,21,22]). By using the Ivantsov solution in these models, it is automatically assumed that the effects due to solutal interactions are negligible. McFadden and Browne [23] discuss this assumption using numerical simulation. The thermal interaction between dendrites is extensive because of the long thermal lengths. However, because of the short solutal lengths, dendritic structures in the early stages of growth can be treated as being solutally isolated. It was proposed that only in the final stages of diffusion-controlled solidification or for high nucleation densities (short distances between dendrites), that we see strong solutal interaction. Other macro models described in literature [24,25]solve the heat transport problem numerically and

then use conservation of solute in the liquid and the Ivantsov solution to determine the growth rate of dendrite tips. An average solute level is assumed to apply to the liquid between dendrites (the region that has been called extradendritic liquid). However, the Ivantsov solution implicitly assumes that the average composition is present at an infinite distance from the solid-liquid interface. Martorano et al. [25] coined the phrase 'solutal blocking' to describe solutal interaction between the columnar and equiaxed zones in castings.

Work has been done to include the effects of convection on the dendrite tip models [26,27,28] where, typically, the authors define a boundary layer around the solid-liquid interface where a modified Ivantsov expression is applied. In the modified Ivantsov the infinite boundary condition is replaced and the nominal composition is set at some finite length, that is, at the boundary layer thickness. Boundary layer theory from fluid mechanics is used determine the thickness of the boundary layer. Recent experimental work has been conducted on transparent alloys to see the effects of convection on a dendrite under settling conditions [29]. It was shown that during sedimentation, orientation and crystal rotation play a role in affecting the dendritic growth rate.

Advances in experimental techniques using synchrotron radiation sources have allowed us to see in-situ metallic alloy solidification for thin-film samples (for example [30,31,32]). These developments are significant for the modelling of solidification in metallic alloys. In the experimental results it is possible to see the extent of the boundary layers of solute around the dendrite crystals. Multiple equiaxed grains have been observed up to the point of impingement [33,34].

This paper presents details of an extended and generalised version of Ivantsov/Horvay-Cahn theory that can be compared to the experimental results available from synchrotron irradiation. Specifically, this model includes a feature to investigate solute build up to levels above the nominal composition at finite distances from the solid-liquid interface. This enables estimation of the growth conditions at the dendrite tip by using experimental measurements of solute levels at finite distances in advance of the tip; thus, overcoming the problem of low resolution at the solid-liquid interface.

It is proposed that this model, in conjunction with future experimental results, can play a role in developing an understanding of length scales in castings, especially in relation to solutal interactions. This model will be useful for all macroscopic (and mesoscopic) models especially when modelling the final stages of solidification. In addition, results from the model may be useful for comparing to results from numerical phase field models.

2. Mathematical Model Details

An ansatz solution is required as part of the mathematical framework. Ansatz solutions are provided in literature. Brener [35], for example, proposed an ansatz for a 3D needle crystal that uses a trigonometric function. Similar to Temkin's approach [36], we use an ansatz solution that uses an integral function. Specifically, the integral function is given as

$$J(\omega, B) = \int_{\omega}^{\infty} \frac{e^{-u}}{\sqrt{u(B+u)}} du \quad (1)$$

where u is an intermediate parameter in the integration process. B is a shape factor, which will be discussed later.

We assume the ansatz solution (interpolation function) for the solute profile in the liquid, c_l, ahead of the dendrite tip, which is of the form

$$c_l(\alpha) = a + b\int_{P\alpha^2}^{\infty} \frac{e^{-u}}{\sqrt{u(B+u)}}du \tag{2}$$

The terms a and b are constants. The problem is defined in terms of parabolic co-ordinates, which is often the case in literature to solve for problems involving a parabolic interface [7,26]. The term α simply describes concentric parabolas and $\alpha = 1$ represents the solid-liquid interface. The parameter P is the solutal Peclet number. At the solid-liquid interface, the composition is given as c_t, hence the boundary condition at the interface described as

$$\alpha = 1,\ \ c_l(\alpha) = c_t \tag{3}$$

Substituting these values into equation (2) gives

$$c_t = a + b\int_{P}^{\infty} \frac{e^{-u}}{\sqrt{u(B+u)}}du \tag{4}$$

Or by substituting with equation (1)

$$c_t = a + bJ(P,B) \tag{5}$$

Another boundary condition is obtained by setting the composition to some level c_f at a finite parabolic coordinate, α_B, ahead of the solid-liquid interface,

$$\alpha = \alpha_B,\ \ c_l(\alpha) = c_f \tag{6}$$

Substituting this boundary condition into equation (2) gives

$$c_f = a + b\int_{P\alpha_B^2}^{\infty} \frac{e^{-u}}{\sqrt{u(B+u)}}du \tag{7}$$

Replacing the integral term with equation (1) yields

$$c_f = a + bJ(P\alpha_B^2, B). \tag{8}$$

To solve for the constant b we subtract equation (8) from equation (5) to get

$$c_t - c_f = b\left(J(P,B) - J(P\alpha_B^2, B)\right) \tag{9}$$

and then rearranging gives

$$b = \frac{c_t - c_f}{J(P,B) - J\left(P\alpha_B^2, B\right)} \tag{10}$$

Substitution of equation (10) into equation (8) gives

$$c_f = a + \frac{(c_t - c_f)}{J(P,B) - J\left(P\alpha_B^2, B\right)} J(P\alpha_B^2, B) \tag{11}$$

and further rearranging develops the expression for the constant *a*

$$a = c_f - \frac{(c_t - c_f)J(P\alpha_B^2, B)}{J(P,B) - J(P\alpha_B^2, B)} \tag{12}$$

We can now substitute for *a* and *b* in equation (2) to get a complete expression for the solute profile in the liquid that satisfies the conditions of equations (3) and (6)

$$c_l(\alpha) = c_f + (c_t - c_f)\frac{J(P\alpha^2, B) - J(P\alpha_B^2, B)}{J(P,B) - J(P\alpha_B^2, B)} \tag{13}$$

By using conservation of solute at the tip, it is known that

$$\frac{dc_l(z)}{dz} = -\frac{V}{D}c_t(1-k) \tag{14}$$

where the derivative at the tip is given in terms of the Cartesian coordinate *z* along the axis of the dendrite, *V* is the growth rate, *D* is the diffusivity of solute species in liquid, and *k* is the partition coefficient.

To find the derivative of the solute profile at the solid-liquid interface, we must obtain a result for the expressions in terms of α. Removal of all terms that do not include α, yields

$$\left.\frac{dc_l(\alpha)}{d\alpha}\right|_{\alpha=1} = \frac{c_t - c_f}{J(P,B) - J(P\alpha_B^2, B)} \left.\frac{\partial}{\partial\alpha}\big(J(P\alpha^2, B)\big)\right|_{\alpha=1} \tag{15}$$

We recognise that we must differentiate the following term with respect to *α*

$$J(P\alpha^2, B) = \int_{P\alpha^2}^{\infty} \frac{e^{-u}}{\sqrt{u(B+u)}}\,du \tag{16}$$

Differentiating under the integral sign using the standard calculus definition gives

$$\left.\frac{\partial}{\partial\alpha}\big(J(P\alpha^2, B)\big)\right|_{\alpha=1} = \frac{-2}{e^P\sqrt{1+\frac{B}{P}}} \tag{17}$$

Substituting back into equation (15) yields

$$\left.\frac{dc_l(\alpha)}{d\alpha}\right|_{\alpha=1} = \frac{-2(c_t - c_f)}{[J(P,B) - J(P\alpha_B^2, B)]e^P\sqrt{1+\frac{B}{P}}} \tag{18}$$

We need to convert from the parabolic coordinate system to the Cartesian system. The conversion for the *z* coordinate is given in terms of the parabolic coordinates *α* and *β* as

$$z = \frac{1}{2}R(\alpha^2 - \beta^2) \tag{19}$$

where R is the tip radius.

By simple differentiation it is shown that

$$\frac{dz}{d\alpha} = R\alpha \tag{20}$$

Applying equation (20) at the tip (where α=1), we have the expression for conservation of solute, equation (14), which can be rewritten as

$$c_t(1-k)V = -\frac{D}{R}\left.\frac{dc_{l(\alpha)}}{d\alpha}\right|_{\alpha=1} \tag{21}$$

Significantly, the choice of ansatz solution determines the composition and composition gradient at the tip. The composition gradients provided from alternative ansatz solutions may be compared to that provided here.

Substituting equation (18) into equation (21) and rearranging we get

$$\frac{c_t-c_f}{c_t(1-k)} = \frac{RV}{2D}e^P\sqrt{1+\frac{B}{P}}\,[J(P,B)-J(P\alpha_B^2,B)] \tag{22}$$

The solutal Peclet number is defined as

$$P = \frac{RV}{2D} \tag{23}$$

The term on the left-hand side of equation (22) is called the supersaturation

$$\Omega = \frac{c_t-c_f}{c_t(1-k)} \tag{24}$$

Typically the supersaturation is given using the original composition c_o instead of c_f, however, authors such as Martorano et al. [25] have demonstrated how the supersaturation can be modified to allow for higher solute levels ahead of the tip. In this analysis, if c_f is replaced with c_o we get the customary form of the equation.

Substituting for the supersaturation and the Peclet number in equation (22) gives

$$\Omega = P\,e^P\sqrt{1+\frac{B}{P}}\,[J(P,B)-J(P\alpha_B^2,B)] \tag{25}$$

Applying a parabolic to Cartesian conversion [26] we have

$$\alpha_B^2 = 1+\frac{2\delta}{R} \tag{26}$$

where δ is defined as the look-ahead distance from the dendrite surface to where the composition was given as c_f. Thus, we have the expression

$$\Omega = P\,e^P\sqrt{1+\frac{B}{P}}\,\left[J(P,B)-J\left(P\left(1+\tfrac{2\delta}{R}\right),B\right)\right] \tag{27}$$

We may call the term on the right hand side a modified Ivantsov solution that has provision for a shape factor B and a finite look-ahead distance δ.

$$Iv(P,\delta,R,B) = P\,e^P\sqrt{1+\frac{B}{P}}\,\left[J(P,B)-J\left(P\left(1+\tfrac{2\delta}{R}\right),B\right)\right] \tag{28}$$

Hence from our initial ansatz assumption, we have a final expression for the dendrite growth law with provision for solute build-up to a level of c_f at a finite distance δ ahead of the tip.

$$\Omega = \frac{c_t - c_f}{c_t(1-k)} = Iv(P, \delta, R, B) \tag{29}$$

To achieve the supersaturation for growth conditions the far-field composition, c_f, must be less than the composition at the tip, c_t.

Figure 1 shows a schematic of the dendrite composition ahead of the dendrite along its *z* axis. Note that the composition at the tip is c_t and declines to some value c_f at a distance δ ahead of the tip.

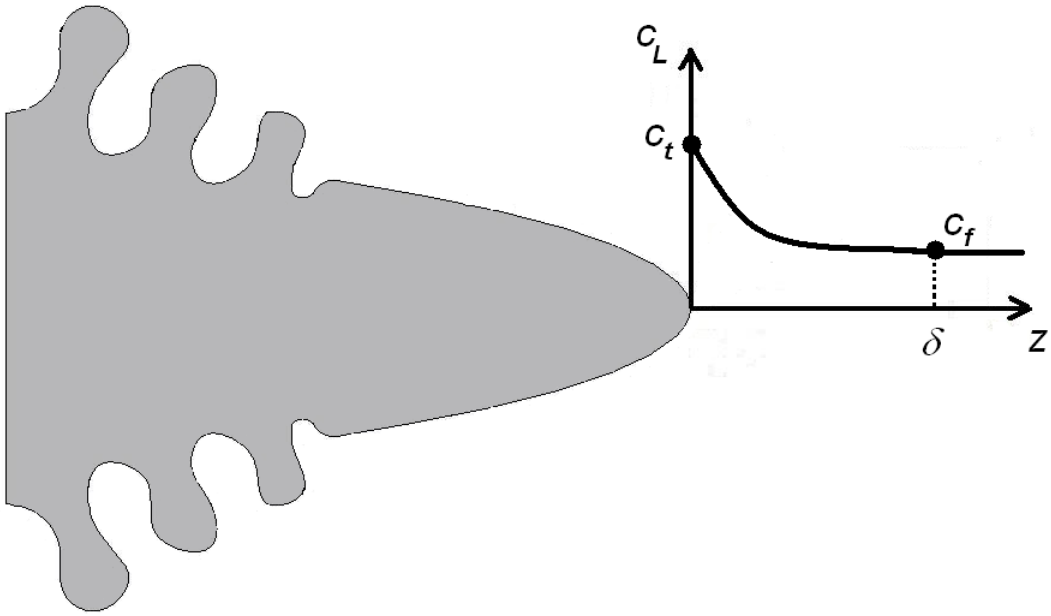

Figure 1: Composition ahead of a dendrite

Horvay and Cahn [7] were the first to define the parameter *B* as shape factor when they used the method of envelope formation. The method outlined in this manuscript is quite distinct from that of Horvay and Cahn. However, in their approach to discussing the problem, Horvay and Cahn showed it was more convenient to describe the problem using the aspect ratio *A*, which is

$$A = \frac{1}{\sqrt{1+B}} \tag{30}$$

The solution for a 2D dendrite plate is given when A = 0. The solution for a 3D paraboloid of revolution is given when A = 1. The solution is for an elliptical paraboloid is given within the range 0 < A < 1. In the following section we discuss further the relationships between equation (29) and the classical solutions to dendrite growth problems given in literature. It is demonstrated that equation (29) is a general solution to the Ivantsov problem. The fundamental assumption with this analysis (and all the Ivantsov theory) is that equation (2) is the interpolation function for the steady-state solute diffusion problem.

To get an expression for undercooling at the dendrite tip we first rearrange equation (29) to get an expression for the composition at the tip

$$c_t = \frac{c_f}{1-(1-k)Iv(P,\delta,R,B)} \tag{31}$$

As is typical in classic dendrite growth theory we need an additional selection parameter for determining the tip radius, *R*, which is

$$R = \frac{\Gamma}{\sigma^*}\left(\frac{1}{2mPc_t(k-1)+GR}\right) \tag{32}$$

where σ^* is the selection parameter, Γ is the Gibbs-Thompson coefficient, *m* is the slope of the liquidus line from the phase diagram and *G* is the temperature gradient. The temperature gradient can usually be ignored because of its small effect on the results (hence *GR = 0*).

Using the relationship from the phase diagram we define the global undercooling, ΔT_T, as the difference between the liquidus temperature (taken at the original composition, c_o) and the tip temperature, T_t.

$$\Delta T_T = T_L(c_o) - T_t \tag{33}$$

Assuming the liquidus is a straight line with slope *m*,. the liquidus temperature is

$$T_L(c_o) = T_M + mc_o \tag{34}$$

where T_M is the melting temperature of the pure solvent element.

The tip temperature is obtained from a similar line adjusted for curvature undercooling, ΔT_R,

$$T_t = T_M + mc_t - \Delta T_R. \tag{35}$$

Generally, the curvature undercooling is given as

$$\Delta T_R = \Gamma\left(\frac{1}{R_1} + \frac{1}{R_2}\right) \tag{36}$$

where R_1 and R_2 are the principal radaii of curvature. However, for the 2D scenario the curvature undercooling is $\Delta T_R = \Gamma/R$ and for the 3D scenario it is given as $\Delta T_R = 2\Gamma/R$. Stefanescu [10] discusses curvature undercooling in more depth.

By using equation (31) for the tip composition and subtracting equation (35) from equation (34) we get the total global undercooling

$$\Delta T_T = m\left(c_o - \frac{c_f}{1-(1-k)Iv(P,\delta,R,B)}\right) + \Delta T_R \tag{37}$$

This new expression for the undercooling is different from that of previous authors in two repects: 1) the modified Ivantsov function is used, and 2) the composition c_f ahead of the dendrite tip which may be higher than c_o is considered.

Alternatively, one can define an expression in terms of local undercooling at the tip, ΔT_t.

$$\Delta T_t = T_L(c_f) - T_t \tag{38}$$

The local undercooling is defined in terms of the composition at the far-field position, c_f, and it is given by the equation

$$\Delta T_t = mc_f\left(1 - \frac{1}{1-(1-k)Iv(P,\delta,R,B)}\right) + \Delta T_R \tag{39}$$

The difference between the global undercooling and the local undercooling is obtained by subtracting equation (39) from (37)

$$\Delta = \Delta T_T - \Delta T_t = m(c_o - c_f) \tag{40}$$

This undercooling is the difference between the global undercooling and the local undercooling measured at a distance δ ahead of the dendrite tip. This difference is due to a solute increase above the original composition measured at δ.

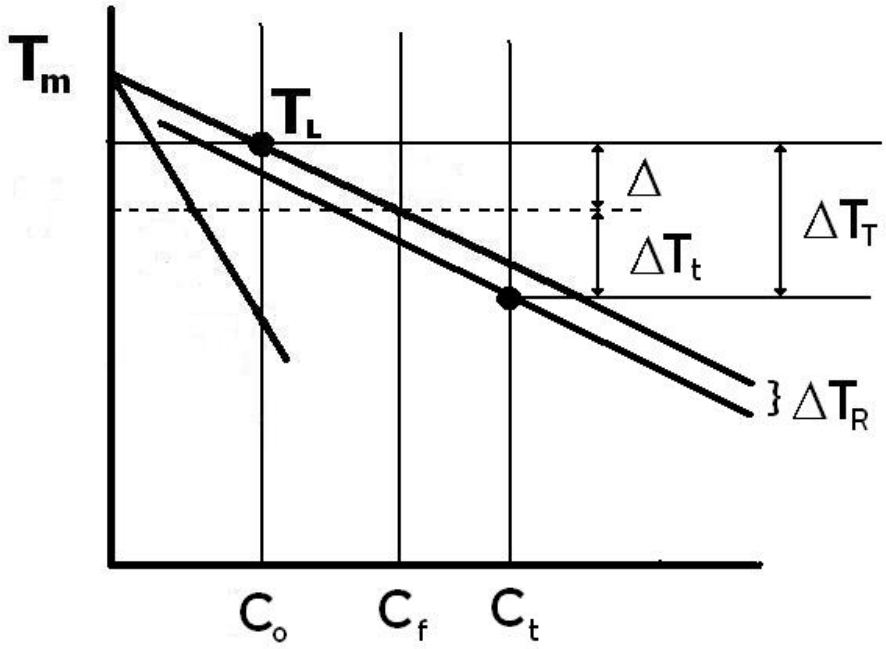

Figure 2: Phase Diagram representation showing the global and local undercooling

Of course when there is no solutal interaction or global solutal enrichment ahead of the dendrites, δ tends towards infinity, c_f is replaced throughout with c_o, and Δ is zero.

The global and local undercoolings are represented on a phase diagram in Fig. 2. Figure 3 shows a schematic representation of the liquidus temperature profile ahead of the dendrite tip. Note that the local undercooling must be measured at the look-ahead distance, δ. Figure 3 shows the constitutional undercooling (shaded part of plot) when the dendrite is growing in a constrained way with a temperature gradient of G imposed at the tip.

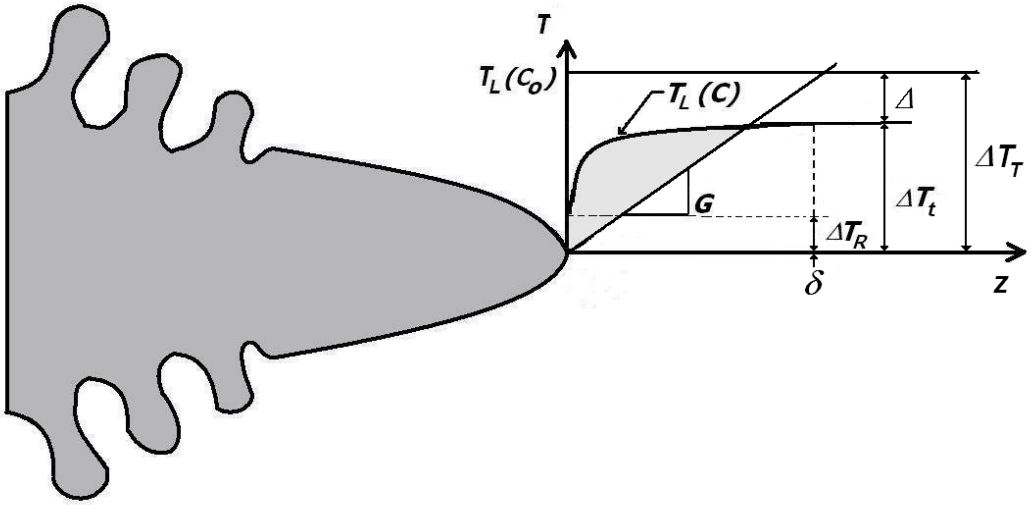

Figure 3: Schematic view of the liquidus temperature and constitutional undercooling ahead of a dendrite tip that is growing in a constrained way

3. Calculation

The analytical model presented here is solved numerically. In this work, the integral expression given in equation (1) is calculated to within a sufficient order of accuracy using a trapezoidal rule. The integrand expression in equation (1) tends to zero as the intermediate variable, *u*, tends to infinity, hence the integration may be truncated. A double iterative scheme is used to solve for the tip radius and growth velocity for a given selection parameter.

4. Discussion on the Generality of the Model

The general nature of the extended Ivantsov function developed here is demonstrated by letting various parameters tend to limiting values.

Our starting point is the general equation for the growth rate

$$Iv(P,\delta,R,B) = \frac{c_t - c_f}{c_t(1-k)} = P\, e^P \sqrt{1+\tfrac{B}{P}}\left[J(P,B) - J\left(P\left(1+\tfrac{2\delta}{R}\right),B\right)\right] \qquad (41)$$

Taking the integral function

$$J(\omega,B) = \int_{\omega}^{\infty} \frac{e^{-u}}{\sqrt{u(B+u)}}\,du \qquad (42)$$

it can be seen that in the limit when B tends to zero we get the exponential integral function used in the original Ivantsov theory

$$\lim_{B\to 0} J(\omega,B) = E_1(\omega) \qquad (43)$$

where

$$E_1(\omega) = \int_{\omega}^{\infty} \frac{e^{-u}}{u} du. \tag{44}$$

Thus, If we set $c_f = c_o$ and let B tend to zero we have

$$\lim_{B\to 0} Iv(P,\delta,R,B) = \frac{c_t - c_o}{c_t(1-k)} = P\, e^P \left[E_1(P) - E_1\left(P\left(1+\frac{2\delta}{R}\right)\right)\right] \tag{45}$$

This expression is used by Gandin et al. [28] and Pines et al. [37] among others.

Next if we let the look-ahead distance, δ, tend to infinity

$$\lim_{\delta\to\infty} J\left(P\left(1+\frac{2\delta}{R}\right), B\right) = 0 \tag{46}$$

From our general expression we see that when δ tends towards infinity our expression tends towards that given by Horvay and Cahn for an elliptical paraboloid [7]

$$\lim_{\delta\to\infty} Iv(P,\delta,R,B) = P\, e^P \sqrt{1+\frac{B}{P}}\, J(P,B) \tag{47}$$

Also as B tends to zero this equation becomes the well-established 3D Ivantsov equation

$$\lim_{\substack{\delta\to\infty \\ B\to 0}} Iv(P,\delta,R,B) = P\, e^P E_1(P) \tag{48}$$

This is the equation for the 3D paraboloid of revolution.

Finally letting B tend to infinity gives the 2D solution as demonstrated next.

First rewriting expression (47) given above in integral form

$$\lim_{\delta\to\infty} Iv(P,\delta,R,B) = P\, e^P \sqrt{1+\frac{B}{P}} \int_P^{\infty} \frac{e^{-u}}{\sqrt{u(B+u)}} du \tag{49}$$

Next, using a change of variables approach, we set a new intermediate parameter *t* instead of *u*, where

$$u = t^2 \tag{50}$$

By differentiating we see that

$$du = 2t\, dt \tag{51}$$

and when *u* is set to the lower integration limit (see integral in equation (49))

$$u = P \tag{52}$$

we have

$$t = \sqrt{P} \tag{53}$$

Similarly at the upper integration limit, as *u* tends to infinity so does the variable *t*.

So by rewriting the expression in terms of *t* gives

$$\lim_{\delta\to\infty} Iv(P,\delta,R,B) = P\, e^{P}\sqrt{1+\tfrac{B}{P}}\ \int_{\sqrt{P}}^{\infty}\frac{e^{-t^2}}{\sqrt{t^2(B+t^2)}}2t\ dt \tag{54}$$

After some rearranging of the term in the denominator of the integrand yields

$$\lim_{\delta\to\infty} Iv(P,\delta,R,B) = P\, e^{P}\sqrt{1+\tfrac{B}{P}}\ \tfrac{2}{\sqrt{B}}\int_{\sqrt{P}}^{\infty}\frac{e^{-t^2}}{\sqrt{1+\frac{t^2}{B}}}dt \tag{55}$$

Recognising that

$$\tfrac{1}{\sqrt{B}}\sqrt{1+\tfrac{B}{P}} = \sqrt{\tfrac{1}{B}+\tfrac{1}{P}} \tag{56}$$

gives

$$\lim_{\delta\to\infty} Iv(P,\delta,R,B) = P\, e^{P}\sqrt{\tfrac{1}{B}+\tfrac{1}{P}}\ 2\int_{\sqrt{P}}^{\infty}\frac{e^{-t^2}}{\sqrt{1+\frac{t^2}{B}}}dt \tag{57}$$

As *B* tend to infinity

$$\lim_{\substack{\delta\to\infty\\ B\to\infty}} Iv(P,\delta,R,B) = P\, e^{P}\sqrt{\tfrac{1}{P}}\ 2\int_{\sqrt{P}}^{\infty}e^{-t^2}\ dt = \sqrt{P}\, e^{P}\ 2\int_{\sqrt{P}}^{\infty}e^{-t^2}\ dt \tag{58}$$

A formal definition of the complimentary error function is

$$erfc(\omega) = \tfrac{2}{\sqrt{\pi}}\int_{\omega}^{\infty} e^{-t^2}\ dt \tag{59}$$

Thus substituting with the complimentary error function gives

$$\lim_{\substack{\delta\to\infty\\ B\to\infty}} Iv(P,\delta,R,B) = \sqrt{P}\, e^{P}\sqrt{\pi}\ \ erfc\left(\sqrt{P}\right) \tag{60}$$

And this is the expression given by Horvay and Cahn for the 2D dendrite.

If we wish to add the look-ahead parameter δ to the 2D solution, we get the expression

$$\lim_{B\to\infty} Iv(P,\delta,R,B) = \sqrt{P}\, e^{P}\sqrt{\pi}\ \left[erfc\left(\sqrt{P}\right) - erfc\left(\sqrt{P\left(1+\tfrac{2\delta}{R}\right)}\right)\right] \tag{61}$$

5. Results and Discussion

Figure 4 shows various interpolated solute profiles for the case where c_t = *11* wt.%, c_f = *10* wt.%, and δ is at infinity. For demonstration, the tip radius has been set to 5 µm and the Peclet number has been set to 0.025. For this discussion it is convenient to discuss the aspect ratio *A* rather than the parameter *B*. Equation (30) describes the relationship between the two parameters. Figure 4 shows a series of solute profiles starting with *A = 1* (or *B = 0*) and stepping down in increments of *0.1* to the value *A = 0* (which is *B* at infinity). As parameter A decreases the composition levels in the profile ahead of the tip increase and the composition gradients at the tip location reduce. It is clear to see

that as A reduces to zero (or B tends towards infinity) the profile converges asymptotically to a final value (i.e., *A*= *0*).

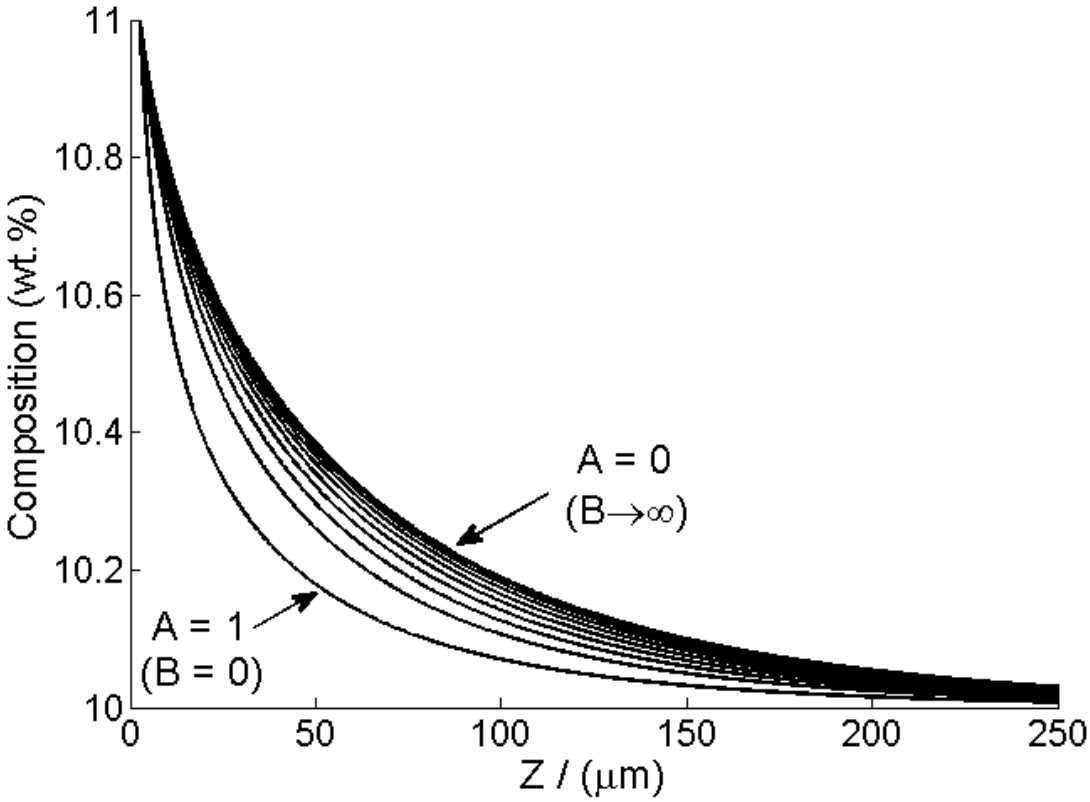

Figure 4: Demonstration of an increasing solute profile due to the shape factor *A* (and *B*)

Next we set a boundary condition of c_f = *10.5* wt.% at a look-ahead distance of δ = 250 μm. Figure 5 shows that, with the new boundary condition, the solute profile has been increased. The solid lines show the original profiles with the infinite look-ahead distance; the broken lines show the solute profiles for the finite look-ahead boundary condition. For completeness we also show the effect of the aspect ratio on the solute profiles. By increasing the solute level at a finite distance we have increased the solute levels ahead of the dendrite tip and we have decreased the solute gradient at the tip position.

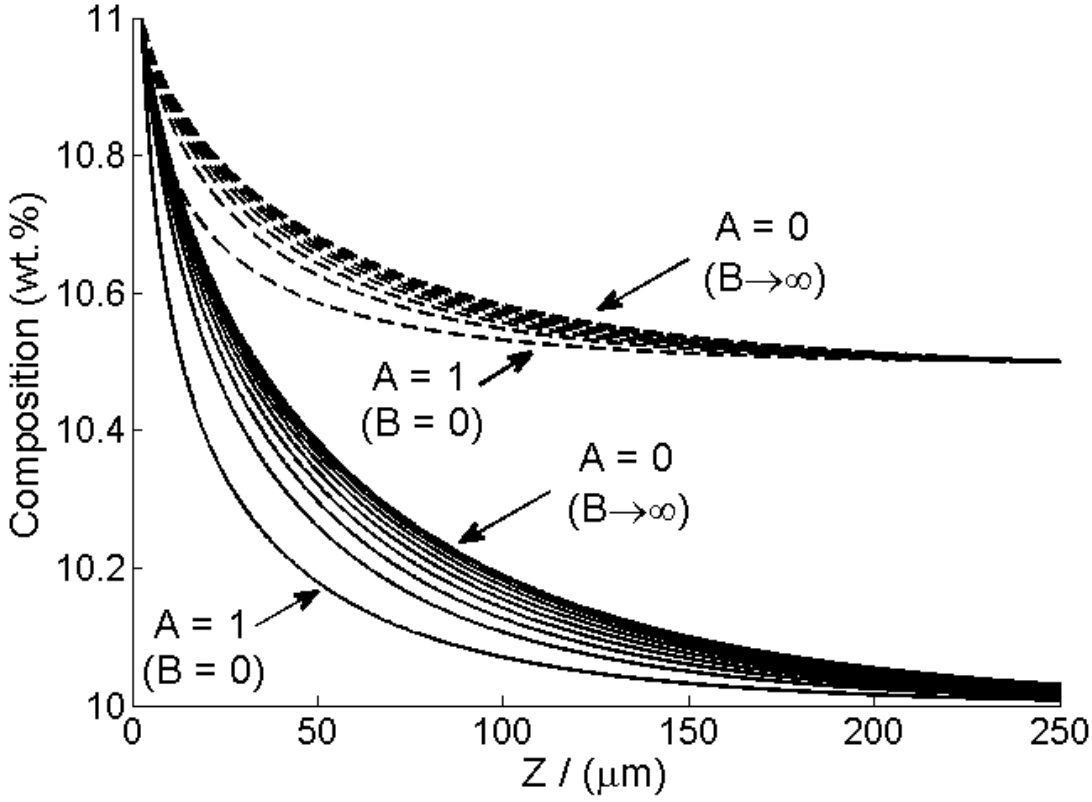

Figure 5: The solid lines are the same as given in figure 4. The broken lines show how the solute profile is changed by setting the far boundary condition at c_f=10.5 wt.% and δ = 250 μm. The effect of shape factor is also shown

The solution for the Peclet number (tip radius and growth rate) and tip composition are solved using a double iterative scheme which iterates firstly on R and secondly on P. Thus, for a given tip undercooling and far-field composition, c_f, at a distance δ ahead of the tip, we solve for P, R, V, and c_t. Throughout the rest of this section the results for all four parameters are plotted against the global undercooling, ΔT_T. The model is demonstrated based on results for an alloy of Al-10Wt.%Cu. Table 1 gives the data used for this alloy. Note that, for demonstration purposes, we have taken the stability parameter as $\sigma^* = 1/4\pi^2$, which is the value given by marginal stability. In this case marginal stability is deemed fit for purpose.

Table 1: Al-10wt.%Cu data

Property	**Value**
Melting Point of Pure Aluminium, T_M	933 K
Liquidus Temperature, T_L	904 K
Slope of the Liquidus Line, m	-2.9 K/wt.%Cu
Gibbs-Thompson coefficient, Γ	1.4 x 10^{-7} mK
Partition Coefficient, k	0.127
Diffusivity of solute in Liquid, D	2.4 x 10^{-9} m^2/s

Figure 6 gives the results for the case where the look-ahead distance is sent to infinity and the look-ahead composition is set to the original composition, that is , $c_f = c_o$. The aspect ratio parameter, A, is

set to three levels, namely, *A* = 1, *A* = 0.9, and *A* = 0. Figure 6(a) shows the Peclet number; figure 6(b), the tip's growth rate; figure 6(c) the tip radius; and figure 6(d), the tip composition all versus global undercooling. Generally, at a given global undercooling, as we decrease A, we decrease the Peclet number and the growth rate. Otherwise as we decrease A, the tip radius increases and the tip composition increases very slightly (only appreciable at the higher undercooling).

The parameter *A* has a strong effect on the growth rate as demonstrated in figure 7. Figure 7 shows the tip growth rate versus global undercooling with the parameter *A* varying between two ranges, specifically, 0.99 ≥ A ≥ 0.91 in steps of 0.01 and 0.9 ≥ A ≥ 0.1 in steps of 0.1. As A tends towards zero we get convergence: for A < 0.6 we see close agreement with solution for A = 0.

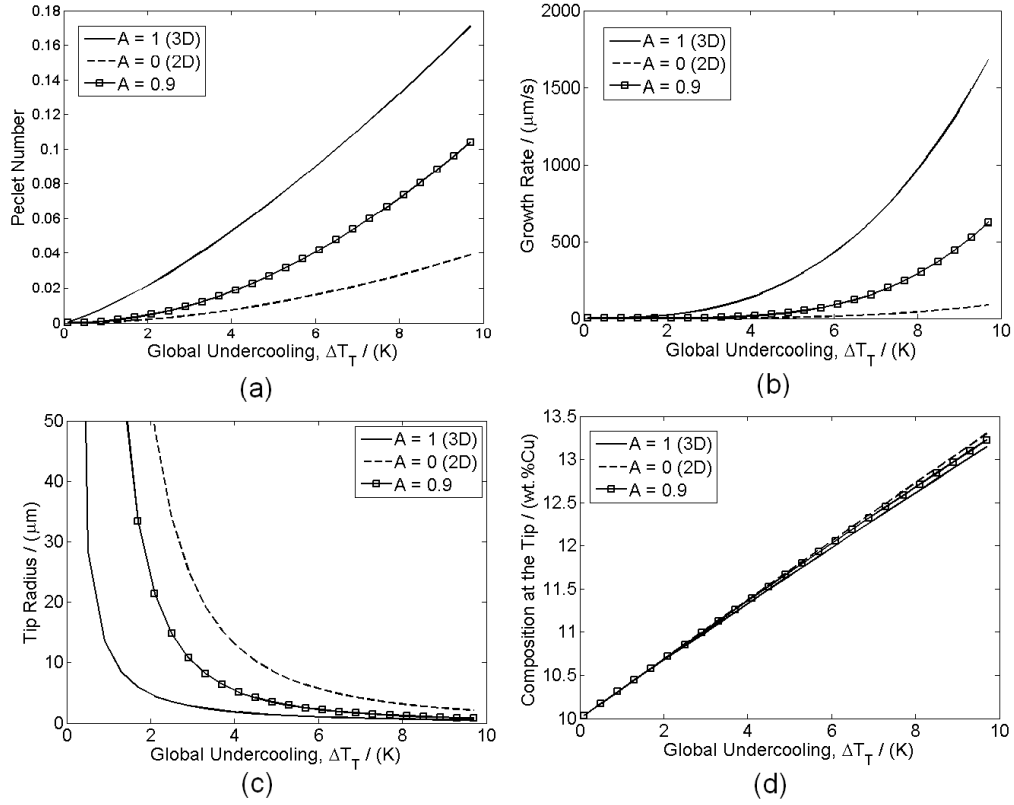

Figure 6: Results for Al-10wt%Cu with $c_f = c_o$, $\delta \rightarrow \infty$, and for three cases of aspect ratio, A = 1, A = 0.9, A = 0.

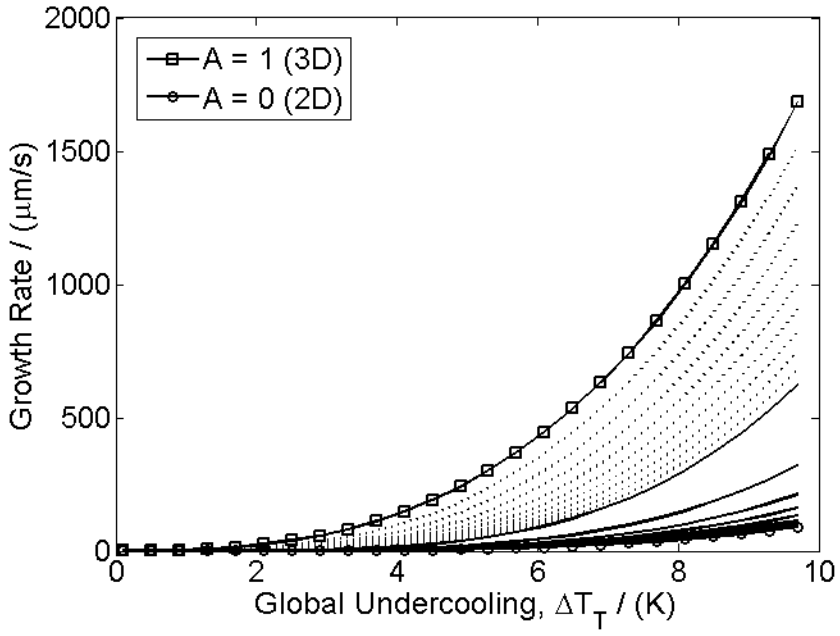

Figure 7: Growth rate versus global undercooling for Al-10wt.%Cu: A = 1 (3D), A = 0 (2D). Dashed lines show results for A in the range 0.99 ≥ A ≥ 0.91 with a uniform step size of 0.01. Solid lines show the results for A in the range 0.9 ≥ A ≥ 0.1 with a uniform step size of 0.1.

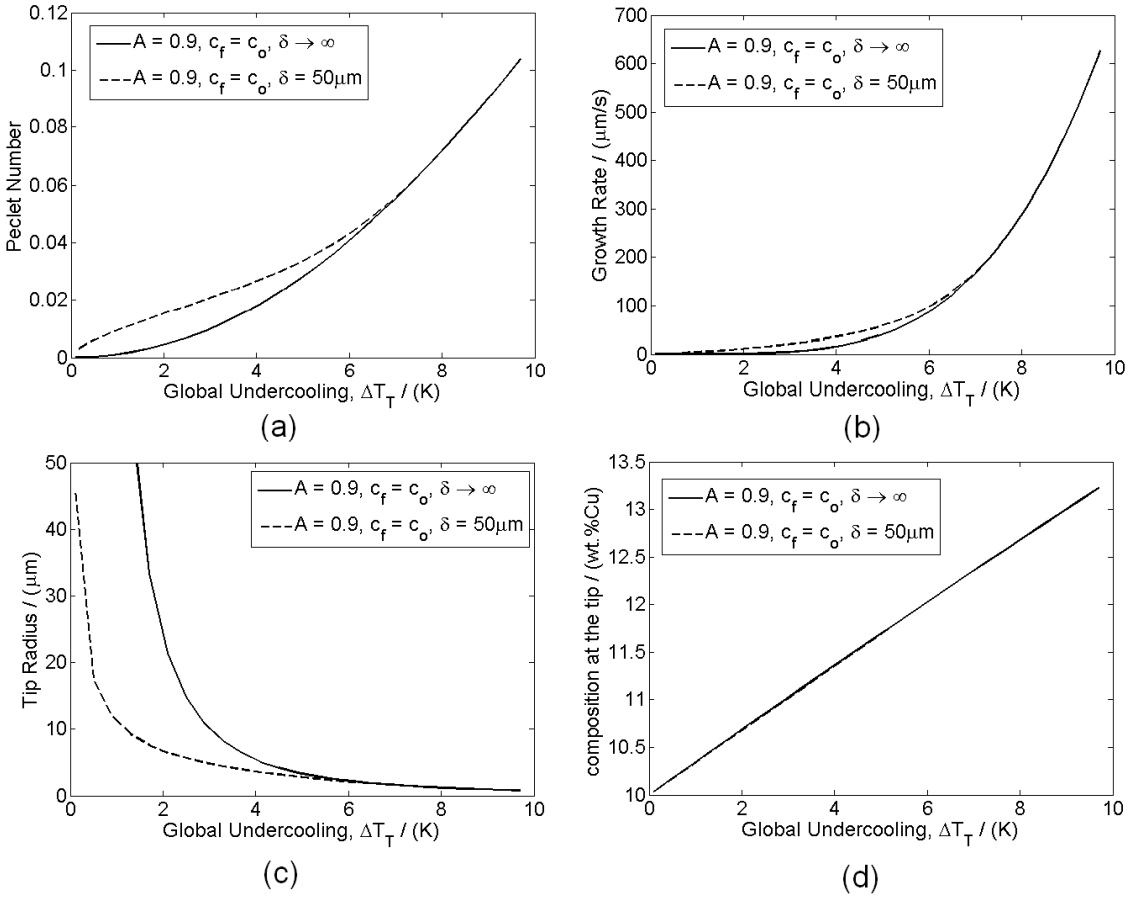

Figure 8: Results for Al-10wt%Cu with $c_f = c_o$, A = 0.9, and two cases look-ahead distance: $\delta \rightarrow \infty$ (solid line) and δ = 50 μm (dashed line).

Figure 8 compares two cases, both with with A = 0.9 and $c_f = c_o$, but one with $\delta \rightarrow \infty$ and the other with δ = 50 µm. We see that by setting the composition to c_o at some finite distance increases the Peclet number (figure 8(a)) and the growth rate (figure8(b)), especially at the lower global undercooling levels. The tip radius is reduced by setting the composition to c_o at a finite δ (figure 8(c)). The composition at the dendrite tip, c_t, is practically unaffected by the change in δ (shown in figure 8(d)). The results for the Peclet number in figure 8(a) are similar to those shown by Gandin *et al.* [28]. At the lower undercooling levels, setting the composition at c_o at some finite distance increases the composition gradient at the tip, thus the growth rate is increased. At the larger undercooling levels (or higher growth rates) the solutal length of the composition profile at the tip is very short: hence the solute profile reaches levels close to c_o after a short distance (<<50 µm) ahead of the tip. Hence, at the higher levels of undercooling, a δ = 50 µm is practically the same as the infinite condition and we see agreement between results in figure 8.

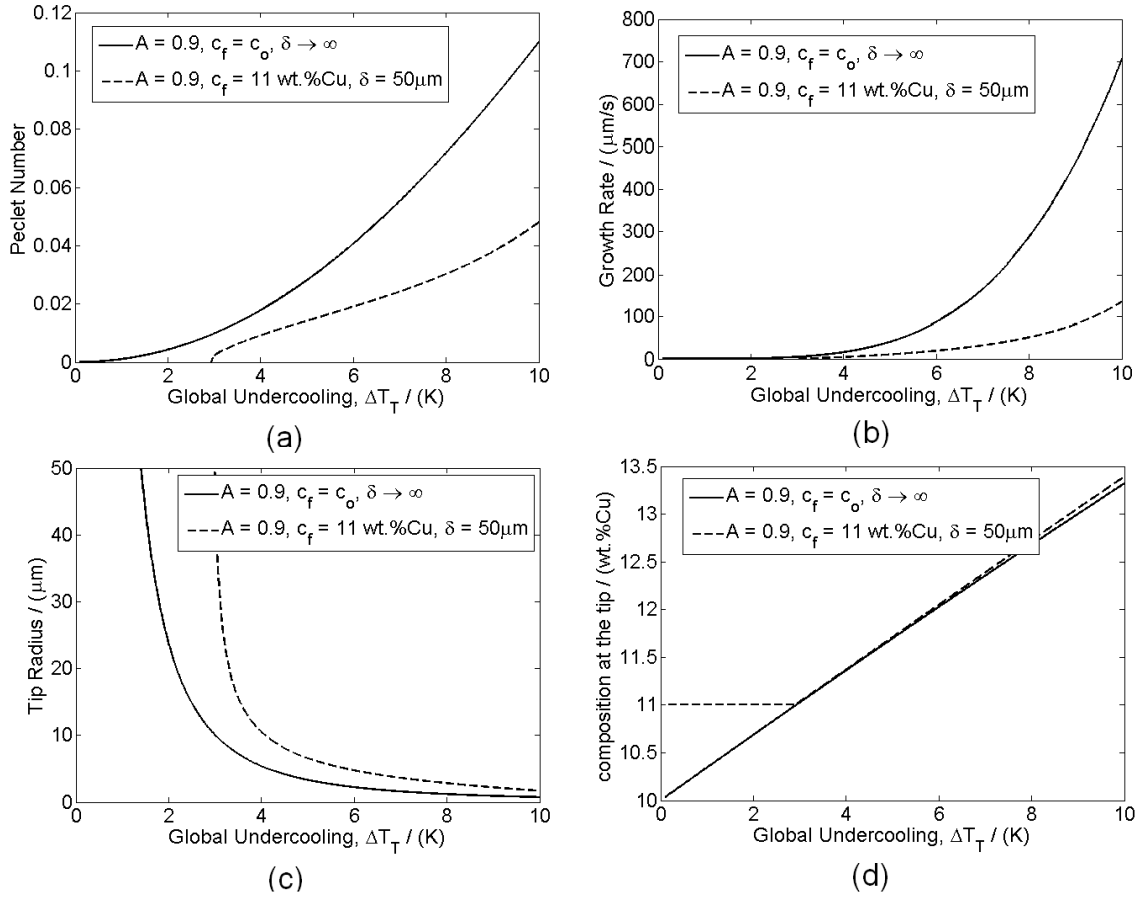

Figure 9: Results for Al-10wt%Cu with A = 0.9 and two cases: $c_f = c_o$ and $\delta \rightarrow \infty$ (solid line), and c_f = 11wt.%Cu and δ = 50 µm (dashed line).

Figure 9 shows two scenarios: one with A = 0.9, $c_f = c_o$ = 10wt.%Cu, and δ at infinity, and the other with A = 0.9, c_f = 11wt.%, and δ = 50 µm. The most significant change brought about by the increase in solute to 11 wt.%Cu is the large reduction in Peclet number (figure 9(a)) and growth rate (figure 9(b)) across all levels of global undercooling. The tip radius (figure 9(c)) is increased when the far-field solute level is increased. Figure 9(d) shows that at low undercoolings, the composition of liquid at the dendrite tip is 11 wt.%Cu, hence, the bath of liquid is uniformly at 11 wt.%Cu and the composition gradient at the tip is zero. It is only above a critical level of global undercooling that we

see dendritic growth conditions. In our example it is at global undercooling levels above 3 K, that we start to see dendritic growth. It is clear to see that the Peclet number is zero at the critical undercooling; hence, the growth rate is also zero. From figure 9(d), it is clear that growth occurs only when the tip composition increases above c_f, thus producing a composition gradient at the tip.

The identification of a critical global undercooling, where the growth rate is zero, is an important novel feature from the newly extended dendrite growth model. It is important to point out that the original Ivantsov formulation can only predict a zero growth rate when the global undercooling is zero; thus, for all global undercooling levels greater than zero, the original Ivantsov model always predicts growth. However, if solute levels are made artificially higher in the liquid around the dendrite, the present model predicts that growth may be prevented at non-zero values of global undercooling. If solute levels are too high and global undercooling is below the critical value, then it is proposed that any existing solid may retreat or melt. Remelting can occur if solute is transported by fluid flow from other liquid regions where solidification is occurring or has occurred. This work only considers the growth kinetics. No discussion on the kinetics of melting (or remelting) is provided. Indeed it should be possible to include a model of melting into the numerical scheme used here, but this is deemed to be beyond the scope of the present manuscript. Rettenmeyr [38] recently provided a review of theory in melting and remelting. Campenalla et al. [39] provide interesting and detailed discussions on remelting in a mushy zone due to solute enrichment by fluid flow. They show that remelting can cause dendrite tips to retreat, but deeper in the mush, remelting may cause fragmentation.

6. Demonstration using Experimental Data

McFadden et al. [40] have demonstrated an application of the current model to data taken from an in-situ synchrotron experiment at the European Synchrotron Radiation Facility. The experiment was performed on a solidifying Al-12wt.%Ge alloy inoculated with TiB_2 for nucleation. The experiment used a Bridgman furnace to investigate the solidification of two impinging equiaxed dendrites. The equiaxed dendrites nucleated at a distance of approximately 700 μm from each other; hence, the length scale of the solidification was less than 1 mm.

Tip growth rates were estimated from the X-ray video sequence. The solute level at the point equidistant from the two impinging dendrite arms (i.e., the midpoint) was measured. Solute levels between the dendrites were observed as solidification proceeded to full impingement.

The generalised dendrite growth model was applied with a selection parameter of $\sigma^* = 1/4\pi^2$ and the aspect ratio parameter was assumed to be unity, i.e., $A = 1$.

A comparison was made between results of the current model and an Ivantsov model of isolated dendrite growth. The results showed that an initial stage of isolated growth (no solutal interaction) was followed by solutal interaction or solutal soft impingement. During the stage of solutal interaction, the growth rates of the dendrite arms were shown to be determined by the local undercooling (equation (38)) and not the global undercooling (equation (33)). Hence the modified model had the advantage that it allowed for a decelerating growth rate with an increasing global undercooling (providing that the local undercooling was diminishing too). Figure 10 demonstrates

this behaviour by showing the levels of global tip undercooling and local tip undercooling versus time for the solidification event reported in [40].

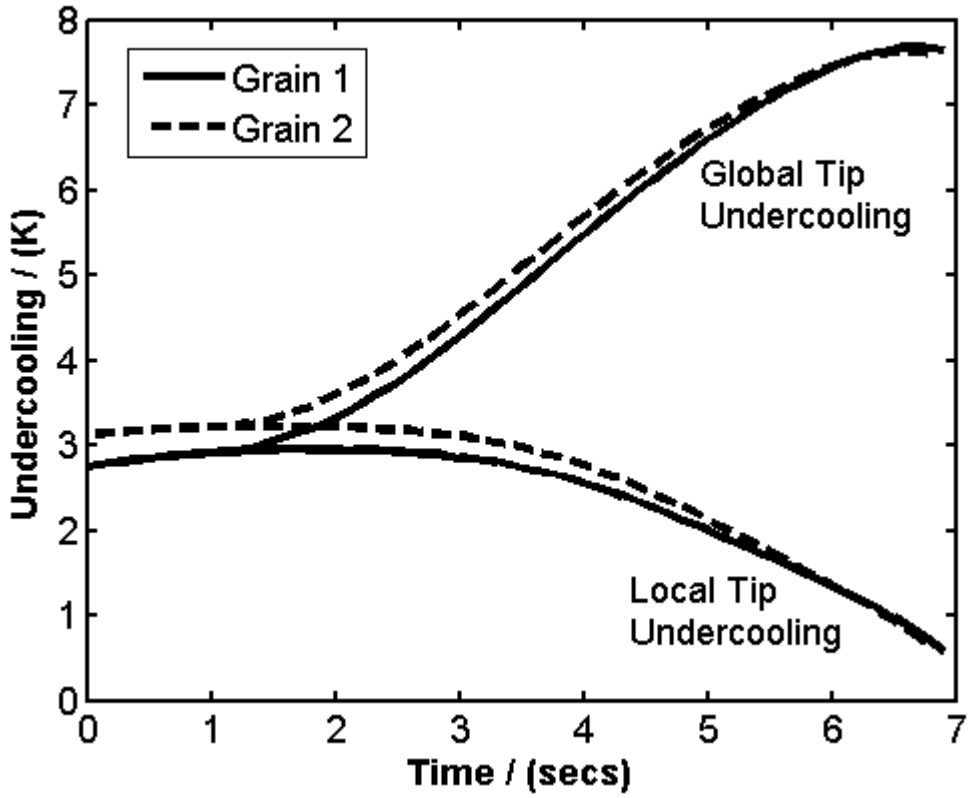

Figure 10: Global tip undercooling and local tip undercooling for an Al-Ge alloy experiment (McFadden et al. [40])

Calculations of the dendrite tip radius were also presented in [40]. The model predicts that the values for the dendrite tip increases as solutal impingement occurs. Further detailed experimental results with measurement of the tip radii are required to determine the suitability of the model in this respect.

7. Conclusion

Mathematical details for a dendrite growth model are presented. The model is developed from the basis of an ansatz solution. The generality of the model is discussed in detail, and specific cases are shown to be consistent with established dendrite growth models that are derived by different methods, namely, Ivantsov [6] and Horvay-Cahn [7]. It is shown that by using the ansatz, it is possible to propose a composition field ahead of the tip by measuring at one coordinate only. A marginal stability criterion is used to determine the operating conditions at a dendrite tip, namely, the growth rate and the tip radius. A unique feature of the model is that it distinguishes between two undercooling levels: the global undercooling, which is based on the nominal composition, and the local undercooling, which is based on the solute composition measured at the coordinate ahead of the tip. The solute composition measured ahead of the tip may be different to the nominal composition. Uniquely, it is shown that for instances where there is a solute build up over the nominal composition ahead of the tip, there may be remelting of the dendrite tip at low, non-zero levels of global undercooling.

The model presented here is useful for investigating experimental, video-microscopy results of alloy dendrite growth viewed using synchrotron radiation. Detailed experimental measurements are required to determine the validity of the model. Specifically, geometrical features such as dendrite tip radius and aspect ratio must be acquired from experiments. In particular, measurements of dendrite tip radii are required to determine the validity of the model in the final stages of solutal impingement.

The aspect ratio of dendrite needs to be measured to establish the relationship between the geometry and solute field around the dendrite. A study of growth in thin films using phase-field modelling may be useful in this respect.

The model will be useful for modellers modelling at various length scales [22,25,41]. For modellers working at the macro and meso scales, this model may be used in a simplified form to get solidification growth rates. In these models it will be important that global conservation of solute is upheld. Other modellers working at the micro scale, such as phase field modellers, may use the new model to verify their results. It is proposed that use of this model in conjunction with specific experiments will assist with the understanding of length scales in castings, especially in relation to solutal interactions.

8. Acknowledgements

The work was funded by European Space Agency (ESA) PRODEX (Arrangement No 4000100805) with the support of the Irish Government and managed by Enterprise Ireland, and by ESA's Microgravity Applications Promotion (MAP) project "In-situ X-ray monitoring of advanced metallurgical processes under microgravity and terrestrial conditions" under contract number 20288/06/NL/VJ. The authors would like to thank Dr. Paul Schaffer and Prof. Ragnvald Mathiesen for providing experimental data. We also would like to express gratitude to Dr. Marek Rebow for providing advice.

9. References

[1] Kurz W. Materials Science Forum 2006;508:313

[2] Trivedi R., Kurz W., International Materials Reviews, 1999;39:49

[3] Laxmanan V., Acta Metallurgica, 1985;33:1023

[4] Huang S.-C., Glicksman M.E, Acta Metallurgica, 1981;29:701

[5] Ivantsov G.P. Doklady Akademiya Nauk SSR, 1947;58:567

[6] Ivantsov G.P. Smithsonian/NASA Astrophysics Data system, 1985: 567-569

[7] Horvay G., Cahn J.W., Acta Metallurgica, 1961;9:695

[8] Lipton J., Glicksman M.E., Kurz W., Materials Science and Engineering, 1984;65:57

[9] Lipton J., Glicksman M.E., Kurz W., Metallurgical transactions A, 1987;18A:341

[10] Stefanescu D.M., Science and Engineering of Casting Solidification (2nd edition),2009, Springer, New York

[11] Langer J.S., Muller-Krumbhaar H., Journal of Crystal Growth, 1977;42:11

[12] Langer J.S., Muller-Krumbhaar H.,Acta Metallurgica, 1978;26:1681

[13] Kessler D.A., Koplik J., Levine H., Phys. Rev. A, 1986;33:3352

[14] Kessler D.A., Levine H., Phys. Rev. Lett., 57 (1986) 3069

[15] Li Q., Beckermann C., J. Crystal Growth, 236 (2002) 482-498

[16] Dantzig J.A. and Rappaz M., Solidification, 2009, EPFL Press, Lausanne, Switzerland

[17] Muschol M. Liu D., Cummins H. Z., Physical Review A, 1992;46

[18] Rebow M., Browne D.J., Scripta Materialia, 2007;56:481

[19] Mullis A.M., Physical Review E 83, 2011, p. 061601

[20] Gandin Ch-A., Acta Materialia, 2000;48:2483

[21] McFadden S. Browne D.J., Gandin Ch.-A., Metallurgical and Materials Transactions A, 2009;

[22] McFadden S. Browne D.J., Applied Mathematical Modelling, 2009;33:1397

[23] McFadden S. Browne D.J., Scripta Materialia, 2006;55:847

[24] Wang C.Y., Beckermann C., Metallurgical and Materials Transactions A, 1993;24:2787

[25] Martorano M.A., Beckermann C., Gandin C.-A., Metallurgical and Materials Transaction A. 2003;34:1657

[26] Cantor B., and Vogel A., Journal of Crystal Growth, 1977;41:109

[27] Schrage D.S., Journal of Crystal Growth, 1999;205:410

[28] Gandin Ch-A., Guillemot G., Appolaire B. , Niane N.T., Materials Science Engineering A, 2003;342:44

[29] Badillo A., Ceynar D., Beckermann C., Journal of Crystal Growth, 2007;309:197

[30] Mathiesen R.H., Arnberg L., Acta Materialia, 2005;53:947

[31]Schenk T., Nguyen-Thi H., Gastaldi J., Reinhart G., Cristiglio V., Mangelinck-Noel N., Klein H., Hartwig J., Grushko B., Billia B., Baruchel J., Journal of Crystal Growth, 2005;275:201

[32] Yasuda H., Ohnaka I., Kawasaki K., Sugiyama A., Ohmici T., Iwane J., Umetani K., Journal of Crystal Growth, 2004;262:645

[33] Bogno A., Nguyen-Thi H., Billia B., Bergeon N., Mangelinck-Noël N., Boller E., Schenk T., Baruchel J. Transactions of The Indian Institute of Metals, 2009;62:427-431

[34] Bogno A., Nguyen-Thi H., Billia B., Bergeon N., Mangelinck-Noël N., Boller E., Schenk T. , Baruchel J., Nuclear Instruments and Methods in Physics Research B, 2009;268:394

[35] Brener E., Phys. Rev. Lett. 1993;71:3653

[36] Temkin D., Acta Materialia, 2005;53:2733

[37] Pines V., Chait A., Zlatkowki M., Journal of Crystal Growth, 1996;167:383

[38] Rettenmeyr M., International Materials Review, 2009;54:1

[39] T. Campanella, C. Charbon, M. Rappaz, Metallurgical and Materials Transactions A., 2004;35A:3201

[40] S. McFadden, P. Schaffer, R.H. Mathiesen, D.J. Browne, Materials Science Forum, 2010;654-656:1359

[41] M. Wu, A. Fjeld, A. Ludwig; Computational Materials Science, 2010;50:32

Figure Captions List

Figure 1: Composition ahead of a dendrite

Figure 2: Phase Diagram representation showing the global and local undercooling

Figure 3: Schematic view of the liquidus temperature and constitutional undercooling ahead of a dendrite tip that is growing in a constrained way

Figure 4: Demonstration of an increasing solute profile due to the shape factor A (and B)

Figure 5: The solid lines are the same as given in figure 4. The broken lines show how the solute profile is changed by setting the far boundary condition at c_f=10.5 wt.% and δ = 250 μm. The effect of shape factor is also shown.

Figure 6: Results for Al-10wt%Cu with $c_f = c_o$, $\delta \rightarrow \infty$, and for three cases of aspect ratio, A = 1, A = 0.9, A = 0.

Figure 7: Growth rate versus global undercooling for Al-10wt.%Cu: A = 1 (3D), A = 0 (2D). Dashed lines show results for A in the range $0.99 \geq A \geq 0.91$ with a uniform step size of 0.01. Solid lines show the results for A in the range $0.9 \geq A \geq 0.1$ with a uniform step size of 0.1.

Figure 8: Results for Al-10wt%Cu with $c_f = c_o$, A = 0.9, and two cases look-ahead distance: $\delta \rightarrow \infty$ (solid line) and δ = 50 μm (dashed line).

Figure 9: Results for Al-10wt%Cu with A = 0.9 and two cases: $c_f = c_o$ and $\delta \rightarrow \infty$ (solid line), and c_f = 11wt.%Cu and δ = 50 μm (dashed line).

Figure10: Global tip undercooling and local tip undercooling for an Al-Ge alloy experiment (McFadden et al. [40])

Table Caption List

Table 1: Al-10wt.%Cu data